Neogenesis and maturation of transient Golgi-like cisternae in a simple eukaryote

Saša Štefanić[1,*,‡], Laura Morf[1,*], Caroline Kulangara[1,§], Attila Regös[1,¶], Sabrina Sonda[1], Elisabeth Schraner[2], Cornelia Spycher[1], Peter Wild[2] and Adrian B. Hehl[2,]**

[1]Institute of Parasitology and [2]Institute of Veterinary Anatomy, University of Zürich, Winterthurerstrasse 266a, CH-8057 Zürich, Switzerland

*These authors contributed equally to this work
‡Present address: Sandler Center for Basic Research in Parasitic Diseases, Mission Bay Campus, University of California San Francisco, San Francisco, CA 94158, USA
§Present address: Swiss Tropical Institute, Socinstrasse 57, 4002 Basel, Switzerland
¶Present address: Institute of Cell Biology, Swiss Federal Institute of Technology Zürich, Schafmattstrasse 18, 8093 Zürich, Switzerland
**Author for correspondence (Adrian.Hehl@access.uzh.ch)

Accepted 23 April 2009
Journal of Cell Science 122, 2846-2856 Published by The Company of Biologists 2009
doi:10.1242/jcs.049411

Summary

The highly reduced protozoan parasite *Giardia lamblia* has minimal machinery for cellular processes such as protein trafficking. *Giardia* trophozoites maintain diverse and regulated secretory pathways but lack an identifiable Golgi complex. During differentiation to cysts, however, they produce specialized compartments termed encystation-specific vesicles (ESVs). ESVs are hypothesized to be unique developmentally regulated Golgi-like organelles dedicated to maturation and export of pre-sorted cyst wall proteins. Here we present a functional analysis of this unusual compartment by direct interference with the functions of the small GTPases Sar1, Rab1 and Arf1. Conditional expression of dominant-negative variants revealed an essential role of Sar1 in early events of organelle neogenesis, whilst inhibition of Arf1 uncoupled morphological changes and cell cycle progression from extracellular matrix export. The latter led to development of 'naked cysts', which lacked water resistance and thus infectivity. Time-lapse microscopy and photobleaching experiments showed that putative Golgi-like cisternae in *Giardia* develop into a network capable of exchanging soluble cargo at a high rate via dynamic, tubular connections, presumably to synchronize maturation. The minimized and naturally pulsed trafficking machinery for export of the cyst wall biopolymer in *Giardia* is a simple model for investigating basic principles of neogenesis and maturation of Golgi compartments.

Supplementary material available online at
http://jcs.biologists.org/cgi/content/full/122/16/2846/DC1

Key words: *Giardia*, Golgi, Regulated secretion, Membrane transport, GTPase, Arf1, Sar1, Cyst wall, Membrane tubule

Introduction

Giardia lamblia (Adam, 2001), an intestinal parasite with worldwide distribution, is a unique model organism to investigate relic organelles (Tovar et al., 2003) and minimal cellular mechanisms (Morrison et al., 2007). Minimal systems in *Giardia* are believed to be mostly the result of reductive processes associated with a parasitic lifestyle (Lloyd and Harris, 2002), but might also reflect some evolutionary basic characteristics (Morrison et al., 2007). The membrane transport system responsible for constitutive and regulated export of surface molecules along multiple pathways lacks an identifiable Golgi complex (Marti et al., 2003a). Consistent with this, most of the machinery for biosynthesis of core N-glycans and all associated quality control modules for endoplasmic reticulum (ER) export are absent (Robbins and Samuelson, 2005; Samuelson et al., 2005). Despite the completely different organization of the trafficking system, a minimal set of universally conserved molecules has been identified (Dacks et al., 2003; Elias et al., 2008; Marti et al., 2003b), suggesting that the basic principles of membrane transport are conserved. During stage-differentiation to infectious cysts, trophozoites synthesize large amounts of cyst wall material (CWM), which is secreted to the surface of the cells in a regulated fashion to form a protective extracellular matrix. The giardial CWM appears to be of very low complexity: only three paralogous cyst wall proteins (CWP1-CWP3) and a simple β1-3 GalNAc homopolymer (Gillin et al., 1996; Jarroll et al., 2001; Lujan et al., 1995b; Sun et al., 2003) polymerize to a highly effective biological barrier on the surface of encysting cells. An epitope-tagged, membrane-anchored high cysteine non-variant cyst protein (HCNCp) (Davids et al., 2006) had been localized to the periphery of encysted cells, possibly at the interface between the plasma membrane and the cyst wall. In vitro, encystation is triggered by environmental cues, for example, low cholesterol concentration and elevated pH (Lujan et al., 1996), leading to de-repression of the genes coding for CWPs (Davis-Hayman et al., 2003). In the ER, CWPs are rapidly sorted from other secretory cargo and partitioned into newly emerging organelles, dubbed encystation-specific vesicles (ESVs), which have no equivalent in proliferating trophozoites (Lujan et al., 1995a; Marti and Hehl, 2003). Encystation takes 20-24 hours in vitro, and ESVs develop to approximately uniform size in the first 8-10 hours, after which they mature and become secretion competent (Marti et al., 2003a). In the absence of constitutive and inherited compartments that could be defined as Golgi cisternae in *Giardia*, ESVs are the only post-ER delay compartments to accommodate the machinery and the cargo for the post-translational maturation processes (Touz et al., 2002) required to produce the CWM. This is supported by circumstantial evidence, such as sensitivity to brefeldin A and recruitment of COPI components and other markers of the secretory system on ESV membranes (Lujan et al., 1995a; Marti et al., 2003b), but direct evidence that ESVs are Golgi analogs is lacking.

The classical Golgi complex is a dynamic organelle system at the center of the secretory pathway in all eukaryotic cells from basal single-celled eukaryotes to mammals (Warren and Malhotra, 1998). In unicellular organisms, Golgi organization is less complex, ranging from unlinked stacks associated with ER exit sites in *Pichia pastoris* (Bevis et al., 2002; Rossanese et al., 1999) and several protozoa (Benchimol et al., 2001; Hager et al., 1999; Struck et al., 2008), to individual, functionally distinct Golgi cisternae without stacked organization in *Saccharomyces cerevisiae* (Rossanese et al., 1999). Microsporidia, intracellular fungal parasites of mammals, have highly reduced trafficking systems, and lack a conventional Golgi (Beznoussenko et al., 2007).

Our working model for ESV neogenesis and maturation during encystation stresses the analogy to the cisternal progression model (Losev et al., 2006), with the important difference that ESVs are not steady-state organelles but arise in response to a pulse of CWM exported from the ER (Marti and Hehl, 2003; Marti et al., 2003a). The process following ESV genesis can be understood as a simultaneous progression (maturation) of ESVs from a *cis* to a *trans* stage concluding with regulated exocytosis of the CWM. Another tenet of this model is that ESV neogenesis has similar requirements as Golgi reconstitution upon mitotic exit in higher eukaryotes or Golgi neogenesis in some protozoa (He et al., 2004). Because both are dependent on membrane transport from the ER to the Golgi, a prediction is that key elements of the early secretory machinery, such as the small Ras-family GTPases Sar1 and Arf1, coat proteins and factors, such as SNAREs, that direct membrane fusion events, are required for ESV formation. Association of a few of these components with compartments of the regulated secretory pathway in *Giardia* has been demonstrated previously (Marti et al., 2003b).

To test the hypothesis that ESVs are minimal, stage-regulated Golgi analogs we investigated the machinery involved in regulated export and maturation of the CWM using a functional approach. The alternative possibility is that ESV genesis is independent of classical ER export machineries but directed by a non-conserved mechanism specific to *Giardia* and linked to the biophysical properties of the CWM, for example a propensity to self-aggregate in ER subdomains. As a first step, we tested whether the genetically conserved key elements of the early secretory pathway – the giardial homologs of the small-GTPases Arf1, Sar1 and Rab1 – are necessary for establishing the regulated pathway for CWM export. We show that the functional requirements for ESV formation are surprisingly conserved despite fundamental differences in compartment organization supporting the analogy of the process to neogenesis of *cis*-Golgi cisternae. We then addressed the question of how maturation of the apparently highly condensed CWM is coordinated among ~30 ESVs. Surprisingly, quantitative analysis of ESV cargo demonstrated that the CWM in mature ESVs is highly fluid and polymerizes only on the cell surface. In addition, analyses of organelle dynamics in living cells revealed that ESVs are not isolated individual organelles, but establish transient physical connections, which allow rapid exchange of CWM.

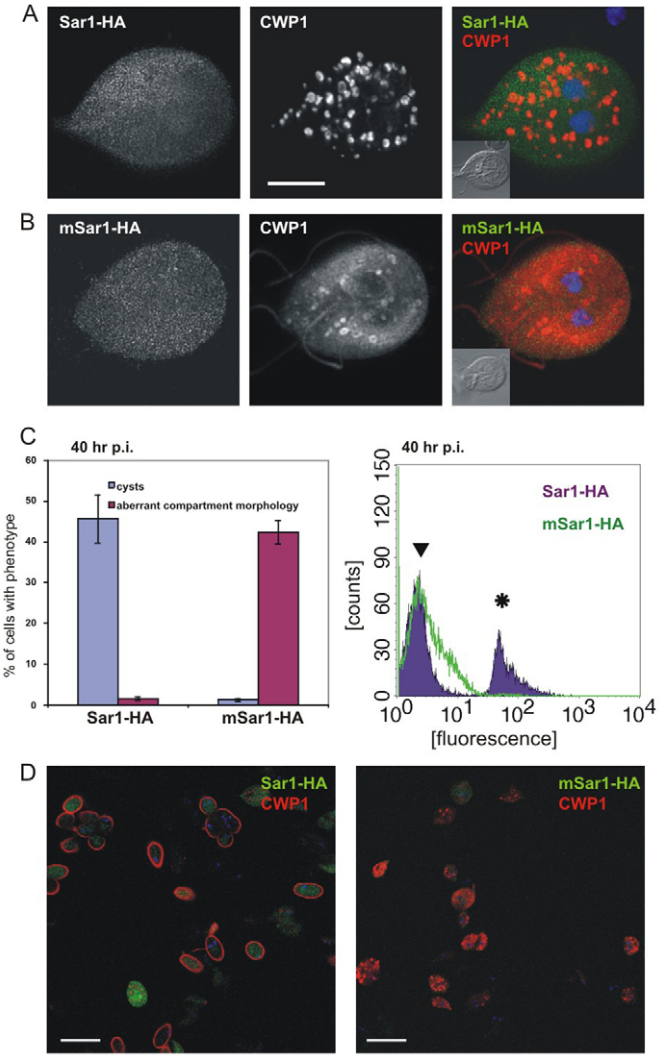

Fig. 1. Giardial Sar1 is necessary for normal ESV development and cyst formation. (A,B) Confocal microscopy of representative cells at 8 h.p.i. expressing high levels of wild-type or mutant (H74G) HA-tagged giardial Sar1 (green). ESVs were detected with a monoclonal antibody against CWP1 (red). Cells expressing the dominant-negative mSar1-HA show aberrant ESV morphology and unspecific secretion of CWP1 to the surface of the trophozoites. Insets: differential interference contrast (DIC) images. Nuclear DNA was stained with DAPI (blue). Scale bar: 5 µm. (C) Left panel: quantification of cyst yields and ESV morphology in cell lines expressing Sar1-HA (control) or mSar1-HA at 40 h.p.i. (endpoint). Results are shown as a percentage (mean ± s.e.m.) of total encysting cells. n=10; P<0.009. FACS analysis of surface-exposed CWP1 in cell populations labeled with anti-CWP1 confirmed manual counts is shown on the right. Note the absence of the cyst peak (asterisk) in mSar1-HA line. Encysting trophozoites (arrowhead). (D) Comparative fluorescence microscopy analysis of detergent-permeabilized cells expressing Sar1-HA or mSar1-HA at 24 h.p.i. Cyst development was abolished in virtually all cells expressing mSar1-HA. Scale bars: 20 µm.

Results

Sar1 function is necessary for ESV and cyst formation

The conserved giardial Sar1 GTPase localizes to ER membranes and putative ER-exit sites in encysting *Giardia* (Marti et al., 2003a), suggesting the involvement of the COPII coat complex in ER export of CWM and establishment of ESV. We tested whether Sar1 was necessary for ER-to-ESV transport in *Giardia* by conditional expression of a dominant-negative variant to generate a Sar1 knockdown. The rationale for choosing this more direct approach rather than mRNA ablation (see also below) was the <20 hour window of opportunity afforded by the only inducible system yielding strong ectopic gene expression currently available (Davis-Hayman and Nash, 2002; Hehl et al., 2000). A short *CWP1* promoter element controls transcription of a gene of interest and is induced in differentiating trophozoites (for direct comparisons of induced

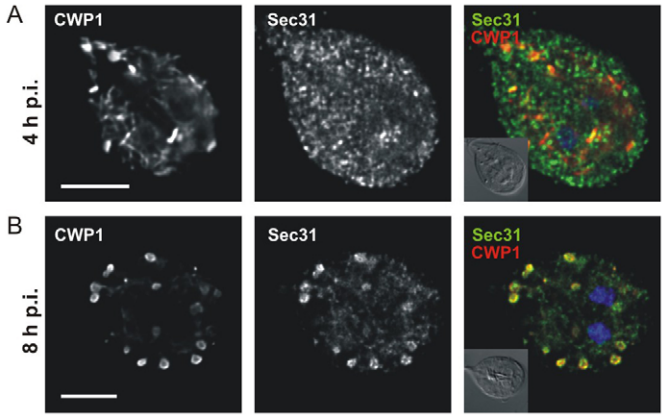

Fig. 2. Localization of the giardial COPII subunit Sec31. Confocal immunofluorescence microscopy analysis of wild-type cells. Specific polyclonal antibodies showed recruitment of COPII coat complex to regions with emerging ESVs at early stages of encystation, 2-4 h.p.i. (A) and 8 h.p.i. (B). Total projections of image stacks are shown. Nuclear DNA is stained with DAPI (blue in merged images). Insets show DIC image. Scale bars: 5 µm.

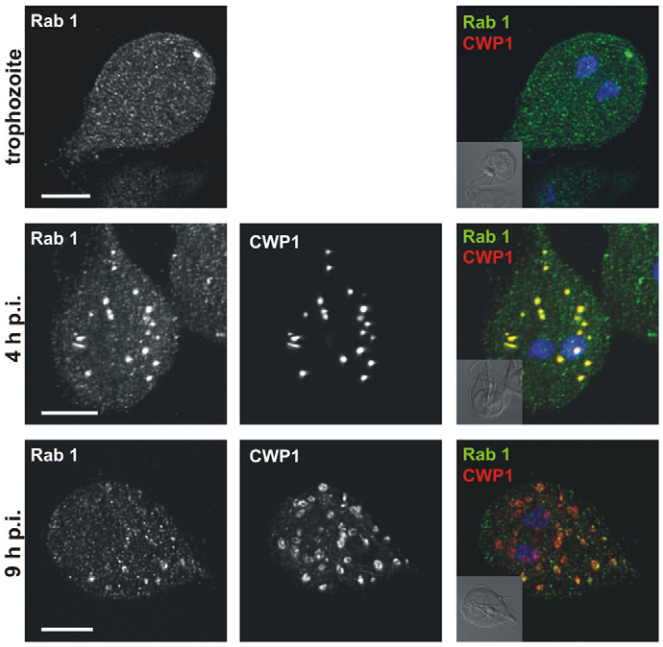

Fig. 3. Giardial Rab1 associates transiently with developing ESVs. Developmentally regulated subcellular localization of Rab1 in proliferating and encysting trophozoites analyzed by confocal microscopy using specific antibodies against the recombinant protein. Rab1 is recruited from a cytoplasmic localization in trophozoites (non induced, top row) to ESV membranes in the first 8 h.p.i. of encystation. In the second phase of encystation (>8 h.p.i.) this association disappears and most of the Rab1 signal is again detected in the cytoplasm. Images show maximum projections of deconvolved image stacks. Insets show DIC image. Scale bars: 5 µm.

recombinant and endogenous GTPases, see supplementary material Fig. S4C). Thus, differentiation, CWM synthesis and export were induced simultaneously with the potentially interfering dominant-negative factor. This is only successful if the effect takes hold early enough to interfere with trafficking. Expression of a *Haemophilus influenza* hemagglutinin (HA)-tagged, mutant Sar1 (mSar1-HA, H74G) with this system resulted in almost complete block of ESV and cyst formation (Fig. 1). Expression of CWPs was induced, but the protein appeared to be dispersed in the ER, in compartments with atypical morphology, and was frequently mistargeted to the surface of trophozoites (Fig. 1B). Quantitative analysis and microscopy confirmed that only ~2% converted to cysts, whereas cells expressing the corresponding wild-type Sar1 showed normal encystation efficiency (~45%) (Fig. 1C,D). This underscored the importance of Sar1-dependent ER export for ESV and cyst formation, and was strong indirect evidence for a crucial role of the conserved COPII heterotetramer in ER export of CWM. Indeed, confocal laser-scanning microscopy (CLSM) analysis of chemically fixed cells using a specific antibody against a giardial Sec31 homolog (supplementary material Fig. S6) showed that this COPII subunit was recruited from the punctate cytoplasmic localization to the vicinity of emerging ESVs (Fig. 2). Similarly to Rab1 (see below), Sec31 lost this specific association as encystation progressed beyond 8 hours post-induction (h.p.i.).

Giardial Rab1 has a role in ESV and cyst wall formation

A role for Sar1/COPII in the export of CWM to ESVs suggested that other conserved key factors of the proximal secretory pathway might be involved in neogenesis of ESVs. A giardial homolog of Yip1 (Heidtman et al., 2003) has previously been localized to early ESV membranes (Stefanic et al., 2006). In higher eukaryotes, this multipass membrane protein was shown to be involved in membrane recruitment of di-prenylated Rab proteins (Yang et al., 1998). Using antibodies against the highly conserved giardial Rab1 (supplementary material Fig. S6), we detected this GTPase transiently on ESV membranes, with maximal recruitment before 8 h.p.i. of encystation (Fig. 3). Similarly to Sec31, Rab1 lost this association in the second half of the 20-24 hour encystation process (Fig. 3), consistent with a function in early secretory transport of CWM and establishment of ESV organelles.

To test the role of Rab1 in encystation, we used conditional expression of an N-terminally tagged 'GTP-locked' mRab1-HA (Q68L). In contrast to cells expressing mSar1-HA, the observed encystation phenotype was not as clear-cut. We observed a significant number of encysting trophozoites (8 h.p.i.) with dispersed CWP signal in immunofluorescence microscopy (Fig. 4A, top row), and a minor proportion (~1-3%) of morphologically normal cysts (i.e. with four nuclei, an oval shape and resorbed flagella) with a strongly reduced or completely undetectable CWP1 signal on the surface (Fig. 4A). The lack of internal CWP1 signal in these cysts suggested that CWM had been secreted or degraded, but was not deposited on the surface. Quantitative analysis of surface-exposed CWP1 on the population level (Fig. 4B) revealed a minor but distinct shift of the cyst peak to the left in cells expressing mRab1-HA compared with the population expressing Rab1-HA, indicating depletion of CWP1 on the surface.

As an independent approach to interfere with Rab1 function during encystation, we attempted ablation of Rab1 mRNA. RNAi in Giardia is controversial (Saraiya and Wang, 2008) and gives inconsistent results. Conditional expression of a Rab1 antisense RNA under the control of the strong CWP1 promoter had no effect (data not shown). However, expression of a Rab1-specific RNA stem-loop (Fig. 4C; supplementary material Fig. S2B,C) resulted in moderately reduced (60-70%) Rab1 mRNA level by quantitative RT-PCR at 4 h.p.i., compared with a slight upregulation in control cells (Fig. 4C). Interestingly, an identical cyst phenotype was

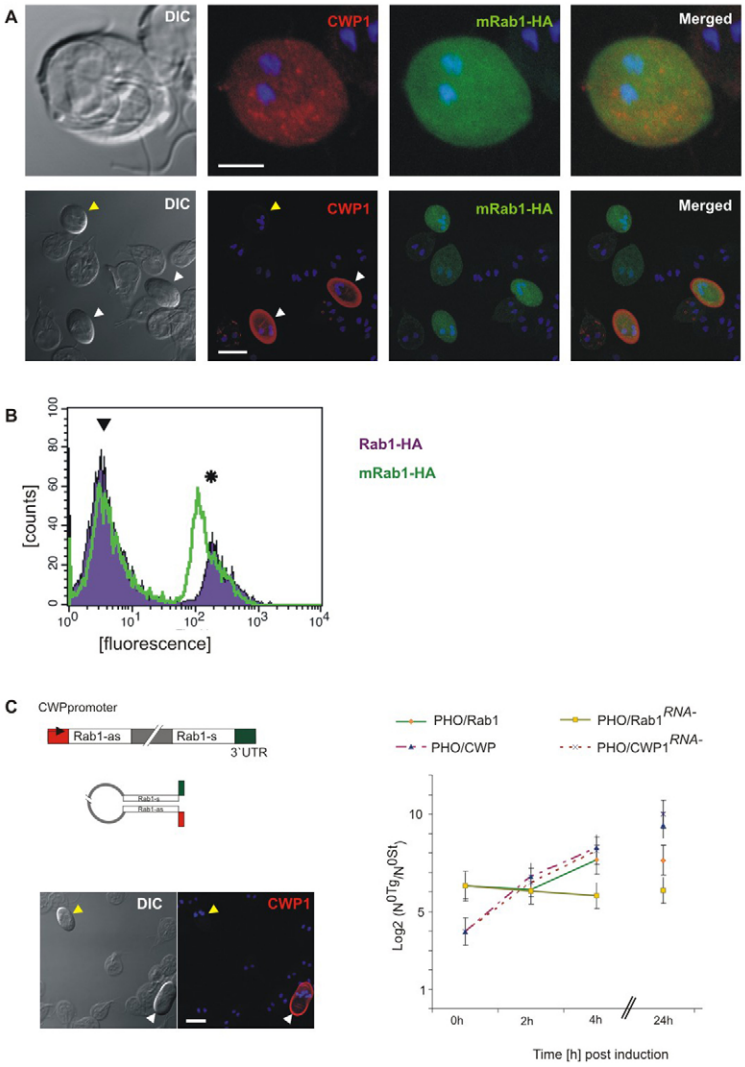

Fig. 4. Rab1 is necessary for ESV development and cyst wall formation. (A) Immunofluorescence microscopy analysis of chemically fixed and detergent-permeabilized cells overexpressing the dominant-negative (Q68L), HA-tagged Rab1 variant mRab1-HA (green). Top row: induced trophozoite (8 h.p.i.) with abnormal distribution of CWP1 (red). Scale bar: 5 µm. Bottom row: cell population at 24 h.p.i. with normal cysts (white arrowheads) and a cyst lacking a CWP1 signal (yellow arrowhead). DIC, differential interference contrast. Scale bar: 10 µm. (B) FACS analysis of cells expressing the wild-type Rab1-HA (purple) or the dominant-negative mRab1-HA (green line) at 24 h.p.i. Surface-exposed CWP1 is detected in unpermeabilized cells. Arrowhead, trophozoites; asterisk, cyst peak. The latter is shifted to the left indicating diminished CWP1 on the surface of many cysts. Cysts lacking CWP1 (Fig. 4A) are probably included in the population of unstained cells (arrowhead). (C) Graphical representation of the stem-loop construct used in mRNA ablation experiments. Red box, CWP1 promoter, gray box, (human Bcl) linker sequence; green box, CWP1 3′UTR. Right panel shows a representative quantitative RT-PCR experiment using mRNA extracted from pooled cells (three biological replicates for each time point). Conditional overexpression of a Rab1-specific stem-loop RNA (left) led to a 60-70% reduction of endogenous Rab1 mRNA levels 4 h.p.i. (PHO/Rab1^{RNA-}) compared with control parasites expressing only the antisense and linker portion of the heterologous RNA (PHO/Rab1). Induction of CWP1 mRNA was equally strong in both cell lines. Bottom left panel shows images of specific phenotype seen in cells after Rab1 mRNA ablation at 24 h.p.i. Morphologically normal cysts in bright-field images show strongly decreased or missing signal after immunostaining of surface exposed CWP1 (yellow arrowhead). White arrowhead indicates a normal cyst. Scale bar: 10 µm.

observed in these cells (Fig. 4C; supplementary material Fig. S2C), albeit with similar low frequency, supporting the notion that this sporadic but consistent phenotype (~1-3% of all cysts) was indeed specific.

Ablation of Arf1 function selectively inhibits cyst wall formation

The small GTPase Arf1 functions as the key regulator of COPI and clathrin membrane coats at Golgi membranes (D'Souza-Schorey and Chavrier, 2006). Transient association of COPI and clathrin coats with early and mature ESVs, respectively, has been demonstrated previously (Marti et al., 2003b). The conserved *Giardia* Arf1 (supplementary material Fig. S1) localizes to punctate structures below the lateral and dorsal plasma membrane, by confocal microscopy, suggestive of an association with the endosomal-lysosomal peripheral vesicle (PV) system (Fig. 5), as observed for giardial clathrin (Gaechter et al., 2008). Arf1 recruitment to ESV membranes in encysting cells is evident at 7-14 h.p.i., which is consistent with the previously observed recruitment of β′-COP and the sensitivity of ESVs to brefeldin A (Hehl et al., 2000; Lujan et al., 1995a).

An essential function of Arf1 in organelle maturation is a central prediction of the Golgi model for ESVs. We tested this using a functional knock-down approach, i.e., conditional expression of a dominant-negative mutant Arf1 (mArf1, Q71L) variant in encysting cells. By initial light microscopy examination, encystation appeared unimpaired in transgenic cells (Fig. 6). Surprisingly, fluorescence microscopy analysis showed that virtually all cyst forms that were positive for mArf1-HA lacked surface-exposed CWP1 (Fig. 6B). However, ESV development appeared normal, which suggested that ER export and partitioning of CWM into ESVs was unaffected (see also supplementary material Fig. S4B).

Controls expressing wild-type Arf1-HA showed complete secretion of CWM and a normal cyst wall (Fig. 6A), whereas cyst forms from the cell line expressing mArf1-HA contained only non-secreted CWP1 in ESV-like organelles (Fig. 6B; supplementary material Fig. S4). Together, this suggests a block in the maturation phase of ESVs, which interferes with their ability to secrete the CWM. Electron microscopy analysis of ultra-thin sections from cysts fixed at 24 h.p.i. confirmed the absence of secreted CWM on these 'naked cysts', despite apparent completion of all other morphological transformations. Quantitative analysis showed a tight encystation phenotype in transgenic cells (Fig. 6C). We also tested whether mutant cysts had lost their resistance to water: a hallmark of bona fide cysts. The 'naked cysts' were completely unprotected and lysed in water, similarly to

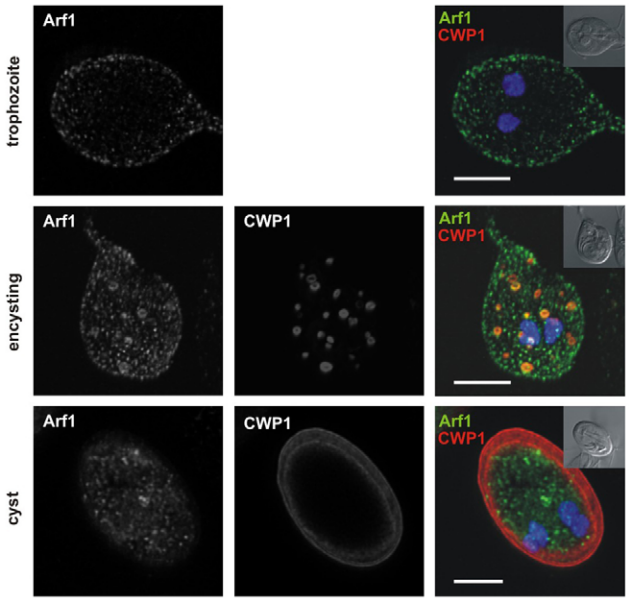

Fig. 5. Subcellular localization of giardial Arf1. Developmentally regulated localization of Arf1 in trophozoites and cysts by confocal microscopy using specific antibodies against recombinant ARF1. In encysting cells at 7-14 h.p.i. Arf1 is clearly recruited to ESVs (middle row). The distribution in uninduced trophozoites is punctate and preferentially near the dorsal plasma membrane (top row), a pattern consistent with labelling of peripheral vesicles similar to the localization of the giardial clathrin heavy chain (Gaechter et al., 2008). Maximum projections are shown. Insets show DIC image. Scale bars: 5 μm.

the previously sensitive trophozoites (supplementary material Fig. S3). Thus, a functional knockdown of Arf1 appeared to decouple cell cycle progression and morphological changes from matrix secretion, suggesting that these coordinated mechanisms are controlled independently during late phase encystation.

ESVs develop into a connected post-ER network of organelles

Functional analysis indicated that ESV neogenesis – formation of morphologically distinct post-ER organelles (Lujan et al., 1995a; Reiner et al., 2001; Stefanic et al., 2006) – is directed by a universally conserved machinery that is also responsible for the genesis of pre-Golgi intermediates and *cis*-Golgi cisternae in higher eukaryotes (reviewed by Stephens and Pepperkok, 2001). ER export of CWM and partitioning into ESVs appears to be completed by 5-8 h.p.i. in our in vitro system; however, ESVs only become secretion-competent just before cyst wall formation at 20-24 h.p.i. A plausible explanation of ESV formation and maturation is the 'pulsed cisternal progression model', where the synchronous maturation of ESVs and cargo is analogous to the *cis* to *trans* maturation of Golgi cisternae (Marti and Hehl, 2003). Because the CWM is secreted quantitatively in only a few minutes, and polymerizes rapidly, key cargo maturation processes (DuBois et al., 2008; Touz et al., 2002) are probably synchronized between the ~30 ESVs in an encysting cell. An elegant solution would be a mechanism allowing direct exchange of CWM between ESVs.

To test whether ESVs are able to exchange CWM during the maturation phase (8-20 h.p.i.), we developed protocols for live-cell imaging by confocal microscopy using a CWP1::GFP reporter shown previously to be exported via ESVs and incorporated into the cyst wall (Hehl et al., 2000). At 10-12 h.p.i. the reporter was typically sequestered in fully formed ESVs (Figs 7 and 8). Transgenic cells were unimpaired in their ability to attach to glass surfaces, which allowed observation in sealed chambers for up to 1 hour. Fluorescence recovery of photobleaching (FRAP) analysis was used to quantify cargo dynamics. Photobleaching of individual organelles resulted in rapid signal recovery, typically reaching a maximum less than 90 seconds after the start of the bleaching cycle (Fig. 7A,B). This was surprising given the highly condensed appearance of the CWM in IFA and EM images. After bleaching of all ESVs in one hemisphere, fluorescence in the target region recovered with similar kinetics (Fig. 7C,D). Quantitative analysis indicated that this recovery was at the expense of the signal in the unbleached half, and the total fluorescence level after 90 seconds stabilized on a significantly lower level. No fluorescence recovery was measured if cells were briefly treated with 1% formaldehyde (data not shown) or if all ESVs in a cell were bleached (Fig. 7E,F). CWP1::GFP was quantitatively secreted with the CWM, and became evenly distributed and completely immobilized (Fig. 7G,H), consistent with polymerization. Taken together the data provide direct evidence for a fully linked ESV organelle network in which the fluid CWM circulate freely. Whether this applies also to CWP2 and CWP3 remains to be determined. An interesting observation was that fluorescence in bleached ESVs never quite recovered to extrapolated levels (see Fig. 7B, asterisk), suggesting that a minor proportion of the reporter was immobilized in ESVs, perhaps forming a condensed core.

Dynamic tubular structures provide the physical link for cargo exchange between ESV compartments

The FRAP experiments suggested that ESVs were immobile at least for the few minutes that these cells were observed. Thus, based on the rapidity of fluorescence recovery, we hypothesized that cargo exchange between ESVs was mediated by permanent or dynamic tubular connections, rather than small COPI- or COPII-coated transport intermediates (Antonny et al., 2001).

To test this, we recorded ESV organelle dynamics for a longer time using time-lapse analysis of attached transgenic cells. Because an ESV-specific membrane marker was not available, the CWP::GFP chimera was used as a luminal reporter for cargo in encysting transgenic cells at 12 h.p.i. The imaging protocol was designed to generate ~1-μm-thick optical sections and to minimize phototoxicity and bleaching. An image series of 100 frames at 21-second intervals (~34 minutes total) showed that ESVs remained stationary in the cell. The movie data also indicated that the organelles undergo considerable change in shape (Fig. 8A,B; supplementary material Movies 1 and 2). However, the resolution of the raw images was insufficient to determine this clearly. To extract the ESV organelle boundaries from background noise, we applied an isosurface function with a fixed threshold value representing organelle boundaries to all frames. This resulted in unbiased models of fluorescence intensity distribution in the time-lapse series (Fig. 8A-C; supplementary material Movie 3) revealing a highly dynamic compartment morphology. Interestingly, the image series suggested the formation and resorption of long tubular structures which dynamically connected ESVs even across cell hemispheres. Previous electron microscopic studies of thin sections suggested a close proximity and even occasional continuity of ER membranes with ESVs (Lanfredi-Rangel et al., 2003). To visualize potential tubular connections between mature ESVs in chemically fixed cells, we used maximum resolution confocal fluorescence microscopy, image deconvolution, and 3D reconstruction. In these

snapshots of cells at >12 h.p.i. labeled with an anti-CWP1 monoclonal antibody, connecting 'channels' as well as blind tubular extensions originating from ESVs were detected (Fig. 8D,E). Interestingly, although difficult to resolve, co-labeling with the ER membrane protein disulfide isomerase 2 (PDI2) showed a clear overlap of signals in some tubular structures (Fig. 8D), raising the possibility that ER membranes might be involved in forming tubular connections between ESVs.

Discussion

Secretory transport requires complex machinery and dynamic compartment organization with the Golgi complex at the center, making study of this system difficult. To address relatively simple questions, for example how cargo moves from the ER through the stack, investigators induce single synchronized traffic waves in mammalian cells (Trucco et al., 2004). Unicellular model organisms, such as *Giardia*, whose trafficking machineries are basic and/or have undergone massive reductive evolution, allow investigation of these fundamental functions in a highly simplified context. Reduction and loss of complexity does not necessarily result in direct reversal of the processes that lead to increasing complexity during eukaryotic evolution. Yet, minimal systems and machineries can extend our view beyond the horizon of the last common eukaryotic ancestor (LCEA) (Dacks and Field, 2007). More importantly, functional analysis of membrane transport systems in *Giardia*, which have a considerably lower complexity than those of the predicted LCEA, could reveal key information about the mechanisms of reductive evolution as a consequence of adopting a parasitic lifestyle. One significant characteristic of the giardial secretory system is the absence of a steady-state Golgi organelle with definable, classically stacked cisternae and faces (Marti et al., 2003a; Elias et al., 2008), which leaves ESVs as the only candidate compartments with a role in post-translational maturation of secretory cargo (Marti and Hehl, 2003). The developmentally regulated genesis of ESVs which are best defined as delay compartments for maturation of a very limited set of pre-sorted secretory material (i.e. CWM) is unique in a highly polarized cell. However, the hypothesis that ESVs are developmentally regulated Golgi analogs that are generated by neogenesis in encysting cells, is difficult to test in the absence of conventional Golgi markers (e.g. GM130, galactosyl transferases or the *trans*-Golgi network marker Rab6) and familiar morphological landmarks. In the present study we therefore focused on predicted functional and structural similarities rather than differences between ESVs in *Giardia* and the Golgi in higher eukaryotes.

ESVs of encysting trophozoites potentially arise by de novo biogenesis, although some form of template structure cannot be excluded. In many higher eukaryotes, Golgi neogenesis is observed after mitotic disassembly and partitioning of Golgi remnants to the daughter cells. However, this mechanism is not universally conserved. The single Golgi stack in the protozoan *Toxoplasma gondii* does not require disassembly (Pelletier et al., 2002), and the Golgi in the forming daughter cell of dividing trypanosomes arises by neogenesis, although it does require some material from the existing Golgi (He et al., 2004). Giardial ESVs are the only known functional Golgi analogs established by de novo biogenesis during stage-differentiation. This is significant in the context of the general simplification and reduction, and/or putative primary basal features in *Giardia*.

In higher eukaryotes the small GTPases Sar1, Rab1 and Arf1 act as molecular switches in this sequence at specific steps during ER export and Golgi transport of secreted proteins (Altan-Bonnet et al., 2004; Aridor et al., 1995). In this study, we interfered with these functions in encysting *Giardia* and elicited distinct phenotypes ranging from failure to progress into stage conversion (Sar1) to a block of cyst wall material secretion (Arf1). Technically, we relied on the conditional expression of dominant-negative mutant variants of the GTPases, which have been used in many different systems to give rise to nonfunctional proteins of the Ras superfamily and block specific functions (Aridor et al., 1995; Dascher and Balch, 1994; Kuge et al., 1994; Lanoix et al., 1999; Memon, 2004; Tisdale et

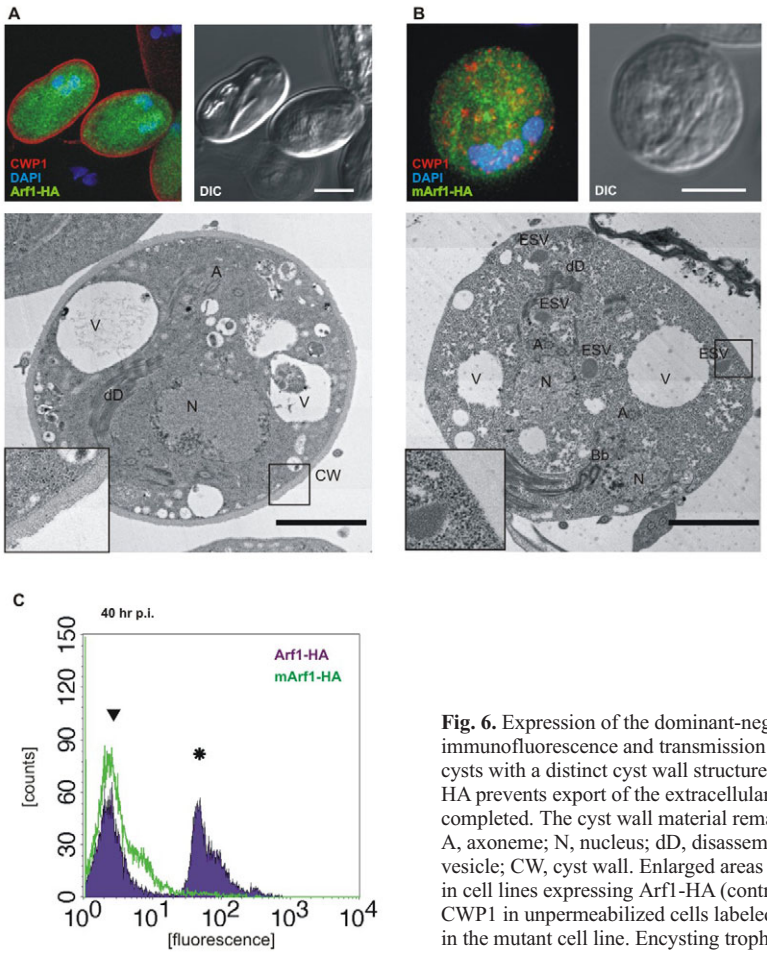

Fig. 6. Expression of the dominant-negative mArf1-HA prevents cyst wall formation. Confocal immunofluorescence and transmission electron microscopic characterization of transgenic cysts. (A) Normal cysts with a distinct cyst wall structure in cells overexpressing wild-type Arf1-HA. (B) Expression of mArf1-HA prevents export of the extracellular matrix, but karyokinesis and morphological transformations are completed. The cyst wall material remains inside. Scale bars: 5 µm (IFA) and 2 µm (tEM). V, vacuole; A, axoneme; N, nucleus; dD, disassembled ventral disk fragment; Bb, basal body; ESV, encystation-specific vesicle; CW, cyst wall. Enlarged areas of the cell surface are shown as insets. (C) Quantification of cyst yields in cell lines expressing Arf1-HA (control) or mArf1-HA at 40 h.p.i. (endpoint). FACS scan of surface-exposed CWP1 in unpermeabilized cells labeled with anti-CWP1. Note the complete absence of the cyst peak (asterisk) in the mutant cell line. Encysting trophozoites (arrowhead).

al., 1992). The well-established conditional expression system controlled by the CWP1 promoter combined with chromosomal integration guaranteed tight repression of these variants in proliferating, and very strong induction in differentiating trophozoites (Hehl et al., 2000). Although interference with functions during early encystation is difficult, this drawback is offset by the tight regulation and the possibility to express lethal genes (Gaechter et al., 2008). By contrast, the only alternative system based on tetracycline-controlled regulation needs 48 hours to produce meaningful amounts of recombinant protein (Sun and Tai, 2000). Post-translational modification (e.g. prenylation) (Calero et al., 2003; Donaldson et al., 2005) required for full functionality of dominant-negative GTPases might delay the inhibitory effect of mutant proteins. For example, by analogy with higher eukaryotes, Sar1 and Rab1 are both expected to be instrumental for early events in ER-to-Golgi transport (Bonifacino and Glick, 2004). However, only interference with Sar1, which does not require post-translational processing, abolished stage-differentiation in most cells, and inhibited ESV formation. This phenotype is consistent with studies using dominant-negative Sar1 in other systems (Aridor et al., 1995; Kuge et al., 1994), and our previous work showing that the giardial cyst wall material is sorted away from constitutively secreted cargo and partitioned into ESVs after its synthesis the ER (Marti et al., 2003a). We detected a sporadic but consistent phenotype of cyst forms that lack CWP on the surface and in internal compartments as a result of mRab1-HA expression or Rab1 mRNA ablation. A possible explanation could be that the phenotype is found only in trophozoites, which respond more slowly to induction. Although distinct developmental stages can be identified easily during encystation, the process has considerable variability. The mRNA ablation approach generally takes longer to produce an effect than expression of a dominant-negative variant. Yet, the requirement for post-translational processing of newly synthesized Rab1 by prenylation probably delays the availability of significant amounts of functional protein. Taken together, this leads to the hypothesis that interference with Rab1 function soon after induction might produce a similarly uniform phenotype as observed for the other GTPases tested here. However, this requires development of a strong and tightly regulated inducible system that is independent of encystation.

Brefeldin A causes the mammalian Golgi to disassemble (Peyroche et al., 1999) and leads to pronounced dispersion of ESVs and blocks cyst formation in *Giardia* (Hehl et al., 2000; Lujan et al., 1995a), suggesting a key role for Arf1 in ESV formation and maintenance. Sorting of CWM into ESVs and organelle morphology were not visibly affected in cells expressing mArf1 variants, but CWM secretion was blocked in almost all encysting cells. This is consistent with a role for giardial Arf1 in essential transport steps between completed establishment of ESVs at 5-8 h.p.i. and exocytosis of CWM at 20-24 h.p.i. Taken together with recruitment of COPI components and the genetic conservation of many other basic components of the trafficking machinery (Marti

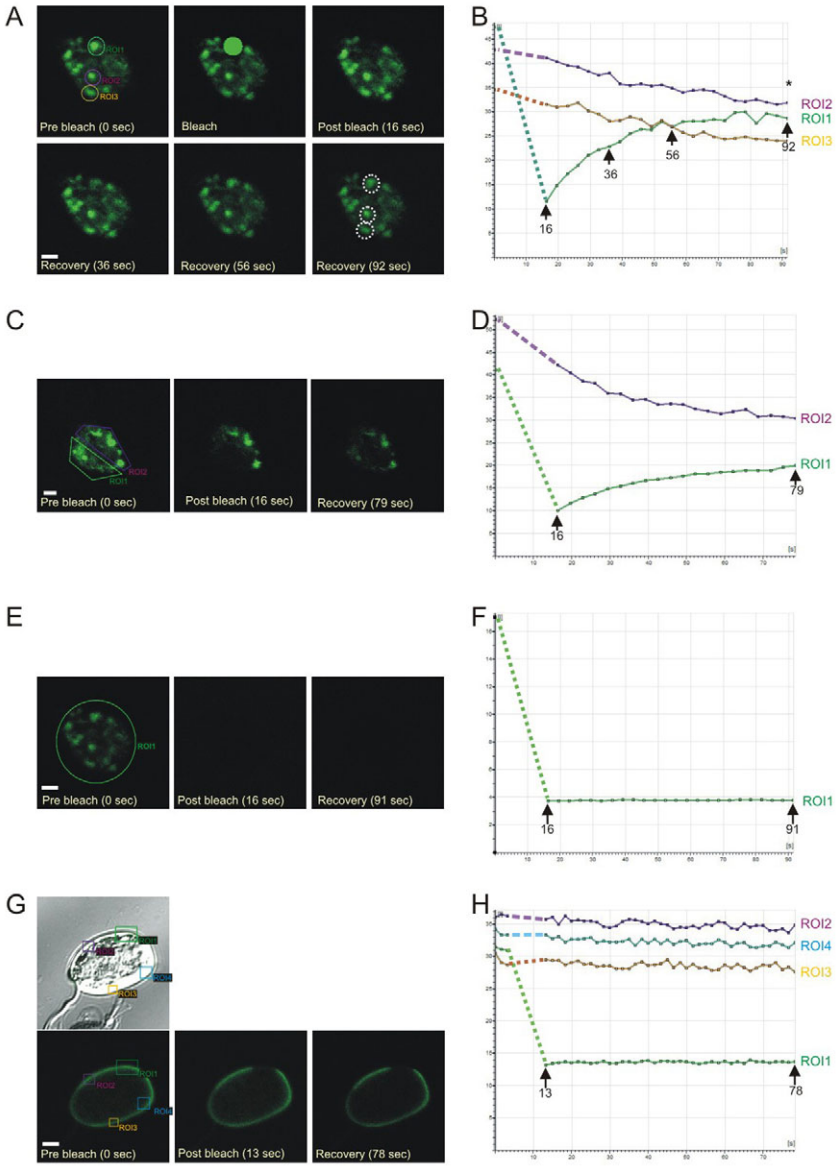

Fig. 7. Fluorescence recovery after photobleaching analysis reveals ESV cargo motility. (A) Single optical sections in a central area of the cell. ESV cargo represented by the CWP::GFP reporter was sequestered almost completely in ESVs with minimal signal observed in surrounding ER structures in a representative attached cell at 12 h.p.i. Region of interest (ROI)1: photobleached organelle. ROI2 and ROI3: control region to assess overall bleaching throughout the experiment (~30%). (B) Quantitative analysis. The signal in ROI1 reaches a plateau at ~75 seconds from the start of the bleaching cycle. Note that the maximal level of recovery in ROI1 is lower than expected based on general bleaching during the imaging process alone (asterisk). Units of fluorescence (*y*-axis) and time in seconds (*x*-axis) are indicated. Time points at which images shown in panels C-F were taken are indicated by arrows. (C,D) Cargo is motile in an ESV network. Photobleaching of all ESVs in one hemisphere (ROI1) of the cell. Recovery of fluorescence in ROI leads to concomitant loss of signal in ROI2. (E,F) No recovery is measured after photobleaching of the entire CWP::GFP pool in ESVs. (G,H) No recovery of fluorescence in a bleached area of the cyst wall (ROI1) is consistent with rapid polymerization of the secreted cyst wall material containing the CWP1::GFP reporter. Scale bars: 2 μm.

et al., 2003b; Morrison et al., 2007), the data support the idea that ESVs develop into analogs of Golgi cisternae.

The requirements and the sequence of events for ESV genesis are remarkably similar to that of early secretory transport leading to *cis*-Golgi formation (Stephens et al., 2000), despite fundamental differences in compartment morphology. However, the exact time when nascent ESVs decouple from ER-exit sites [where sorting of CWM occurs (Marti et al., 2003b)] and assume Golgi characteristics is difficult to pinpoint. Punctate structures that are strongly enriched in Sec31 are observed in close proximity to ESVs (Fig. 2B) up to 8 h.p.i. In the second phase of encystations, this marker disassociates from ESVs together with Rab1 and is replaced with Arf1, β′-COP (Marti et al., 2003b), and later also clathrin (Gaechter et al., 2008). Even though this is consistent with emergence of ESVs from ER-exit sites and development to bona fide Golgi-like post-ER compartments, the physical separation of the ER and ESVs is not clear. EM data (Lanfredi-Rangel et al., 2003) suggest that continuities even with mature ESVs are a possibility. However, resident proteins of both compartments, such as PDIs, BiP and CWPs, are clearly separated. In support of distinct compartment identities, BiP has been shown to cycle through ESVs, from where it is retrieved by the C-terminal ER-retention-signal KDEL (Stefanic et al., 2006). If this signal is mutated, a recombinant BiP distributes evenly in ER and ESVs.

The boundaries between the ER and mature ESVs remain imprecise because of the extensive and dynamic linkage of ESVs by tubular membrane connections. We propose that exchange of cargo and membrane material ensures simultaneous maturation of ESVs. The CWM is sequestered in ~30 fully developed ESVs for the last 10-14 hours of encystation and undergoes post-translational maturation before being exocytosed in a few minutes and polymerizing on the surface. This requires coordination between organelles, presumably by allowing cargo to distribute inside an ESV network structure to ensure that all secreted CWM is fully mature and functional. The nature of these transport intermediates is less clear, however, but probably involves large tubulovesicular rather than small spherical membrane carriers (e.g. classical COPI vesicles). One scenario for the genesis of these connections is that they are formed from ESV membrane material analogous to mechanisms for Golgi ribbon formation (Trucco et al., 2004; Griffiths, 2000; Beznoussenko et al., 2007). Formation of such higher-order compartment structures in cells of mammals, plants and insects is thought to lead to more uniform distribution of processing enzymes. However, key factors involved in Golgi ribbon formation, such as GM130 or GRASPs (Feinstein and Linstedt, 2007; Feinstein and Linstedt, 2008) cannot be identified in the *Giardia* Genome Database, suggesting that this machinery is not universally conserved in eukaryotes. An alternative scenario is that maturing ESVs recruit tubular ER structures to establish inter-organelle connections or maintain connections with specialized subdomains of the ER for the purpose of exchanging cargo. This scenario is supported by co-labeling of CWP in tubular structures with the ER marker. Distinguishing between these two possibilities to explain this novel phenomenon is directly linked to the nature of ESVs as putative Golgi analogs. Despite accumulating evidence for this idea, the current data does not allow us to determine with certainty whether ESVs should be considered specialized ER subdomains, ER-Golgi intermediate compartments, bona fide Golgi cisternae, or, more likely, all of the above at different stages of development. Addressing this question requires a thorough analysis of the discrete ER-exit sites (ERES) in *Giardia* and their role in CWM export. Indeed, preliminary experiments using epitope-tagged Sec23 indicate that ESVs are nucleated by export of CWM at closely associated ERES but become rapidly independent as they accumulate cargo (A.B.H. and Christian Konrad, Institute of Parasitology, University of Zurich, Switzerland, unpublished). This constitutes strong evidence for the Golgi character of ESVs but does not exclude the possibility of an intimate association with some ER domains that persist throughout the encystation process.

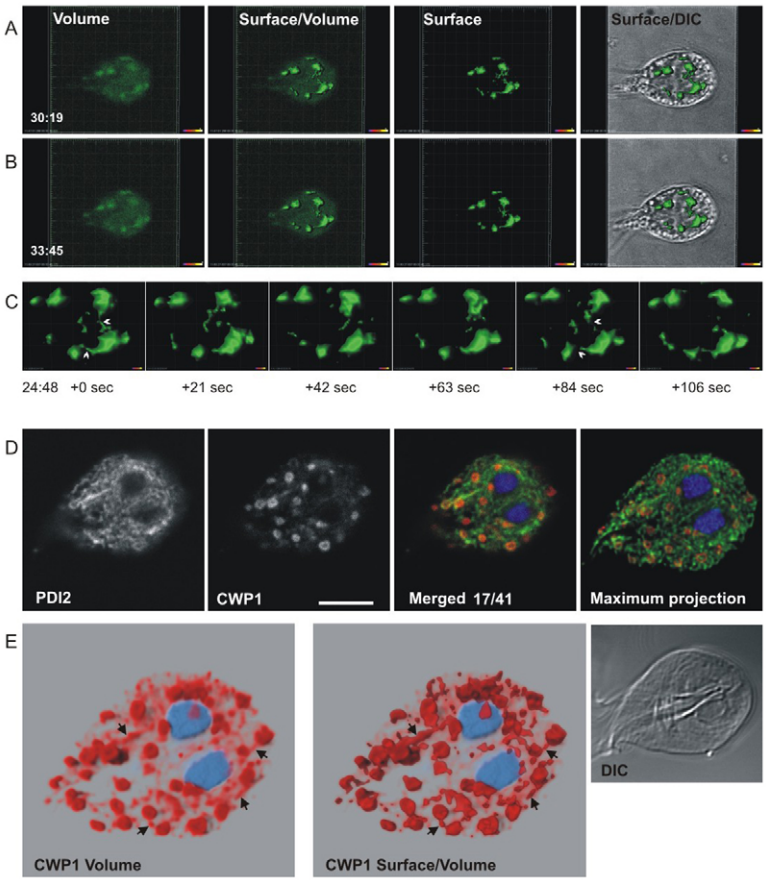

Fig. 8. Dynamic tubular connections between ESVs contain cargo material. (A,B) Time-lapse series of transgenic cells: rows show single frames of the 100 frame sequence (34 minutes total). Isosurface rendering of raw images (left) was used to model organelle boundaries. Differential interference contrast (DIC) images show morphological features of the cell. See also supplementary material Movies 1-3. (C) Isosurface model of six frames documenting organelle dynamics during 106 seconds starting at 24 minutes 48 seconds. Arrowheads indicate dynamic connections between ESV organelles. (D) Confocal microscopy of the secretory system in a representative chemically fixed cell at 12 h.p.i. Antibodies against protein disulfide isomerase 2 (PDI2) and CWP1 represent the ER and ESV compartments, respectively. A single optical section (section 17 of 41), and a maximum projection of the deconvolved image stack is shown. (E) Volume (left image) and surface rendering (middle image) of the CWP1 signal in the entire image stack. Arrows indicate tubular structures with sufficient signal strength to appear in the surface model. A DIC image of the cell is shown on the right. Nuclear DNA is stained blue with DAPI. Scale bars: 5 μm.

Materials and Methods

Culture media, cells and transfection

Trophozoites of the *Giardia lamblia* strain WBC6 (ATCC catalog number 50803) were grown in 11 ml culture tubes (Nunc, Roskilde, Denmark) containing TYI-S-33 medium supplemented with 10% adult bovine serum and bovine bile according to standard protocols (Hehl et al., 2000). Plasmid vector DNA was linearized using *Swa*I restriction enzyme and 15 μg digested plasmid DNA was electroporated (350 V, 960 μF, 800 Ω) into trophozoites. Linearized plasmid targets the *Giardia lamblia* triose phosphate isomerase (*TPI*) locus (see below) and integration occurs by homologous recombination under selective pressure with the antibiotic puromycin (Sigma) (Jimenez-Garcia et al., 2008).

Parasites were harvested by chilling the culture tubes on ice for 30 minutes to detach adherent cells, and collected by centrifugation at 1000 ***g*** for 10 minutes. Cells were then resuspended in phosphate-buffered saline (PBS) and counted using the improved Neubauer chamber.

Encystation was induced using the two-step method as described previously (Hehl et al., 2000), by cultivating the cells for 44 hours in medium without bile and subsequently in medium with higher pH and porcine bile.

Expression vector construction

All constructs were based on the expression cassette C1-CWP for inducible expression under the control of the CWP1 promoter (Hehl et al., 2000). Giardial Sar1, Arf1 and Rab1 (GenBank accession numbers are listed in supplementary material Table S2) coding regions were amplified by PCR from genomic DNA and cloned into *Nsi*I and *Pac*I sites of the C1-CWP vector containing the hemagglutinin (HA) epitope tag upstream of the *Nsi*I restriction site, as described previously (Stefanic et al., 2006), or in the identical vector variant without an HA tag. Single amino acid mutations in the GTPase domains of Sar1, Arf1 and Rab1 were introduced by site-directed mutagenesis (supplementary material Table S1, mutated codon is shown in bold letters). The chimeric CWP1::GFP reporter used in the study was described previously (Hehl et al., 2000). For this study, it was subcloned into the pPacV-Integ vector for chromosomal integration (supplementary material Fig. S5) (Jimenez-Garcia et al., 2008). The pPacV-Integ expression vector for stable integration was designed as a double cassette with a constant part containing a bacterial puromycin-resistance gene under the control of the *Giardia* glutamate dehydrogenase gene promoter (*GDH*, GenBank accession number M84604). Genes of interest including promoter sequences were cloned into adjacent *Xba*I and *Pac*I restriction sites upstream of *CWP1* 3′ flanking sequences. The puromycin-resistance gene and the expression cassette were in head-to-head orientation. Targeting to the intergenic region adjacent to the triose phosphate isomerase gene locus (*TPI*, Giardia DB GL50803-93938) is facilitated by flanking regions (GL50803-17200 and GL50803-93938, respectively), amplified from genomic DNA of *Giardia lamblia* strain WBC6 using corresponding primer pairs (see supplementary material Table S1), digested and ligated between the *Cla*I and *Xba*I restriction sites of the pBluescript KS(–) vector (Stratagene, La Jolla, CA).

Antibody production

The open reading frames of Sar1 (aa 7-189), Rab1 (aa 1-212) and Arf1 (aa 1-191) were PCR-amplified, digested with *Eco*RI, *Pst*I (Sar1), *Xba*I, *Hin*dIII (Arf1) or *Bam*HI, *Sal*I (Rab1), and inserted downstream of the maltose-binding protein (MBP) in plasmid vector pMal-2Cx (New England Biolabs, MA). The fusion proteins were produced in transgenic *Escherichia coli* by induction with 0.5 mM IPTG (isopropyl-β-D-thiogalactopyranoside) for 2 hours at 37°C. MBP fusions were isolated from bacterial lysates by affinity purification on amylose resin according to the manufacturer's protocol (New England Biolabs, MA), dialyzed and lyophilized. NMRI mice were immunized intraperitoneally with 100 μg of fusion protein emulsified with RIBI adjuvant (Corixa, Hamilton, MT) on days 0, 15, 30 and 50. Blood from the tail vein was collected before the initial immunization and after the second and third boost. The serum fraction was assayed for the presence of specific antibodies by western blot (supplementary material Fig. S6) using separated total *Giardia* trophozoite lysate and by IFA (immunofluorescence assay). Only sera reacting with a single, specific band of the expected size were used for assays.

Protein analysis

Giardia parasites were harvested for gel electrophoresis by chilling culture tubes in ice and centrifugation at 1000 ***g***. The cell pellet was washed once in ice-cold phosphate-buffered saline (PBS) and counted in a Neubauer chamber. The cell pellet was dissolved in SDS sample buffer to obtain 2×10^5 cells in 50 μl and boiled for 3 minutes. Dithiothreitol (DTT) was added to 7.75 μg/ml before boiling. SDS-PAGE on 12% polyacrylamide gels and transfer to nitrocellulose membranes was done according to standard techniques. Nitrocellulose membranes were blocked in 5% dry milk, 0.05% TWEEN-20 in PBS and incubated with polyclonal antibodies against Sar1 (1:400), Sec31 (1:200), Rab1 (1:300) and Arf1 (1:500) in blocking solution. Bound antibodies were detected with horseradish-peroxidase-conjugated goat anti-mouse IgG (Bio-Rad, Hercules, CA), respectively, and developed using Western Lightning Chemiluminescence Reagent (PerkinElmer Life Sciences, Boston, MA). Data collection was done in a MultiImage Light Cabinet with AlphaEaseFC software (Alpha Innotech, San Leonardo, CA) using the appropriate settings.

Immunofluorescence microscopy

Cells were harvested by cooling and centrifugation at 1000 ***g*** for 10 minutes. Fixation and preparation for fluorescence microscopy was done as described previously (Marti et al., 2003a). Briefly, cells were washed with cold PBS and fixed with 3% formaldehyde in PBS for 40 minutes at 20°C, followed by a 5 minute incubation with 0.1 M glycine in PBS. Cells were permeabilized with 0.2% Triton X-100 in PBS for 20 minutes at room temperature and blocked overnight in 2% BSA in PBS. Incubation of all antibodies was done in 2% BSA, 0.2% Triton X-100 in PBS. Titrated polyclonal antibodies raised against giardial Sar1, Sec31, Rab1 and Arf1 were incubated for 1 hour at room temperature. Alexa Fluor 488-conjugated secondary antibodies were used as 1:200 dilutions and incubated under same conditions (Molecular Probes, Eugene, OR).

Mouse monoclonal Alexa Fluor 488-conjugated anti-HA (Roche Diagnostics, Manheim, Germany; dilution 1:30) or Cy3-conjugated anti-CWP1 (Waterborne, New Orleans, LA; dilution 1:80) were incubated for 1 hour at 4°C. Washes between incubations were done with 0.5% BSA, 0.05% Triton X-100 in PBS. Labeled cells were embedded with Vectashield (Vector Laboratories, Burlingame, CA) containing the DNA intercalating agent 4′-6-diamidino-2-phenylindole (DAPI) for detection of nuclear DNA. Immunofluorescence analysis was performed on a Leica SP2 AOBS confocal laser-scanning microscope (Leica Microsystems, Wetzlar, Germany) a glycerol objective (Leica, HCX PL APO CS 63×, 1.3 Corr). Image stacks were collected with a pinhole setting of Airy 1 and twofold oversampling. Image stacks of optical sections were further processed using the Huygens deconvolution software package version 2.7 (Scientific Volume Imaging, Hilversum, The Netherlands). Three-dimensional reconstruction, volume and surface rendering were done with the Imaris software suite (Bitplane, Zurich, Switzerland).

Flow cytometric analysis

For quantification of cyst yield in cells expressing giardial Sar1 and Arf1 mutant variants, parasites were induced to encyst for 20 or 40 hours. Cysts and detached trophozoites were collected from confluent cultures by pouring off the culture medium in another tube and rinsing the culture tube twice with prewarmed PBS (37°C). Cells were pelleted by centrifugation at 1000 ***g*** for 10 minutes and processed following the protocol for immunofluorescence (see above) without a permeabilization step. Cysts were fluorescently labeled for 1 hour at 4°C using monoclonal Cy3-conjugated anti-CWP1 antibody (Waterborne, New Orleans, LA; dilution 1:80). Before FACS analysis, cells were washed twice in PBS. Unlabeled samples were used to determine background fluorescence, and subsequently, fluorescently labeled cysts were analyzed in triplicate on a FACSCalibur flow cytometer (Becton & Dickinson, Basel, Switzerland).

For quantification of the mutant Rab1 phenotype, attaching trophozoites and cysts from a culture at 24 h.p.i. were separated by collecting the culture supernatant. Cysts and were collected by centrifugation at 1000 ***g*** for 10 minutes and washed in PBS. Samples were processed and analyzed as described for Sar1 (see above). All samples were analyzed in parallel by IFA to assess encystation efficiency and quality of separation of cysts from trophozoites.

Water treatment of cysts

Cells were induced to encyst (as described above) for 24 hours. The cysts were harvested as described, resuspended in PBS and counted using bright-field microscopy. One half was incubated in 1 ml water, the other with 1 ml PBS overnight at 4°C and counted again. To verify counting, the cells were then fixed and processed for IFA as described above. Statistical analysis was performed using the Comprehensive Meta Analysis software (Version 2.2.046, Biostat, Englewood, NJ).

Gene silencing by RNA ablation

For Rab1 mRNA ablation, a vector for conditional expression of a stem-loop Rab1 double-stranded RNA under the CWP1 promoter was constructed (Fig. 4C). The Rab1 sequences were amplified from genomic DNA using oligonucleotide primers shown in supplementary material Table S1. The Rab sequences were cloned head to head and separated by 750 bp of the human Bcl gene as a spacer. A control construct containing only the antisense sequence of Rab1 followed by the Bcl-linker sequence was used.

RNA isolation and cDNA synthesis

Total RNA was isolated using the Rneasy Mini Kit Qiagen (Qiagen, Hilden, Germany) including a DNase digest (DNase Kit Qiagen). First-strand cDNA synthesis was performed according to standard protocols using an anchored oligo-dT primer and 50 U SuperScript II reverse transcriptase (Invitrogen, Carlsbad, CA). The reaction was incubated at 45°C for 50 minutes and heat inactivated at 70°C for 15 minutes, chilled on ice and followed by digestion with 10 U RNase H for 20 minutes at 37°C.

Quantitative RT-PCR

The standard curves for the iCycler (Bio-Rad) to calculate the slope of each primer pair was generated with Rab1, CWP1, protein phosphatase 1 (PHO) dilutions in duplicate (10^{-2}, 10^{-3}, 10^{-4}, 10^{-5}) using the following cycling conditions: 15 minutes 94°C, 15 seconds 94°C, 20 seconds 58°C, 30 seconds 72°C. PHO mRNA is not regulated during differentiation. PCR amplification was done in triplicate for each

time point and primer pair (PHO-s-quant, CWP1-s-quant, Rab1-s-quant, k-adaptor) (see supplementary material Table S1).

Efficiency was calculated using the equation $e=10^{(-1/slope)}$. The ratio of standard (PHO, CWP1) to target (Rab1) (est×nst/etg×ntg, where est, efficiency of the standard; etg, efficiency of the target; nst, cycle number of the standard at threshold; ntg, cycle number of the target at threshold) was calculated using the Gauss error function. Percentage induction was calculated by setting the Rab1 mRNA level at time point 0 hour to 50%. Levels of CWP mRNA at 24 h.p.i. were set to 100%.

Live-cell microscopy and FRAP analysis

For live-cell microscopy, induced cells expressing the CWP1::GFP chimera were harvested at 12 h.p.i. and transferred to 24-well plates at a density of 6×10^6/ml. After incubation on ice for 5-8 hours, oxygenated cells were sealed between microscopy glass slides and warmed to 21°C or 37°C. Under these conditions, the encysting cells were stable and even continued to complete encystation. For FRAP and time-lapse series, images were collected on a Leica SP2 AOBS confocal laser-scanning microscope (Leica Microsystems, Wetzlar, Germany) using a 63× water immersion objective (Leica, HCX PL APO CS ×63, 1.2 W Corr). The pinhole was set to Airy 2 to increase the thickness of the optical sections to accommodate an entire ESV in the *z*-plane. Quantifiable criteria for cell viability were active attachment to substrate and continuous beating of the ventral and anterolateral flagella pairs. FRAP experiments were performed as described (Gaechter et al., 2008) using the Leica FRAP software module to set bleaching parameters and quantify fluorescence recovery. Movies and surface rendering of raw time-lapse series were generated using the Imaris software suite (Bitplane, Zürich, Switzerland).

We are grateful to Therese Michel for excellent technical assistance and to Norbert Müller for advice with Q-PCR. This study was supported by the Swiss National Science Foundation (Grant no. 3100A0-112327), fellowships from the Stiftung für Forschungsföderung of the University of Zürich and the Roche Research Foundation to C.S., and the Marie-Heim Vögtlin Foundation and Mercier Foundation to S. Sonda.

References

Adam, R. D. (2001). Biology of Giardia lamblia. *Clin. Microbiol. Rev.* **14**, 447-475.

Altan-Bonnet, N., Sougrat, R. and Lippincott-Schwartz, J. (2004). Molecular basis for Golgi maintenance and biogenesis. *Curr. Opin. Cell Biol.* **16**, 364-372.

Antonny, B., Madden, D., Hamamoto, S., Orci, L. and Schekman, R. (2001). Dynamics of the COPII coat with GTP and stable analogues. *Nat. Cell Biol.* **3**, 531-537.

Aridor, M., Bannykh, S. I., Rowe, T. and Balch, W. E. (1995). Sequential coupling between COPII and COPI vesicle coats in endoplasmic reticulum to Golgi transport. *J. Cell Biol.* **131**, 875-893.

Benchimol, M., Ribeiro, K. C., Mariante, R. M. and Alderete, J. F. (2001). Structure and division of the Golgi complex in Trichomonas vaginalis and Tritrichomonas foetus. *Eur. J. Cell Biol.* **80**, 593-607.

Bevis, B. J., Hammond, A. T., Reinke, C. A. and Glick, B. S. (2002). De novo formation of transitional ER sites and Golgi structures in Pichia pastoris [comment]. *Nat. Cell Biol.* **4**, 750-756.

Beznoussenko, G. V., Dolgikh, V. V., Seliverstova, E. V., Semenov, P. B., Tokarev, Y. S., Trucco, A., Micaroni, M., Di Giandomenico, D., Auinger, P., Senderskiy, I. V. et al. (2007). Analogs of the Golgi complex in microsporidia: structure and avesicular mechanisms of function. *J. Cell Sci.* **120**, 1288-1298.

Bonifacino, J. S. and Glick, B. S. (2004). The mechanisms of vesicle budding and fusion. *Cell* **116**, 153-166.

Calero, M., Chen, C. Z., Zhu, W., Winand, N., Havas, K. A., Gilbert, P. M., Burd, C. G. and Collins, R. N. (2003). Dual prenylation is required for Rab protein localization and function. *Mol. Biol. Cell* **14**, 1852-1867.

D'Souza-Schorey, C. and Chavrier, P. (2006). ARF proteins: roles in membrane traffic and beyond. *Nat. Rev. Mol. Cell Biol.* **7**, 347-358.

Dacks, J. B. and Field, M. C. (2007). Evolution of the eukaryotic membrane-trafficking system: origin, tempo and mode. *J. Cell Sci.* **120**, 2977-2985.

Dacks, J. B., Davis, L. A., Sjogren, A. M., Andersson, J. O., Roger, A. J. and Doolittle, W. F. (2003). Evidence for Golgi bodies in proposed 'Golgi-lacking' lineages. *Proc. Biol. Sci.* **270 Suppl. 2**, S168-S171.

Dascher, C. and Balch, W. E. (1994). Dominant inhibitory mutants of ARF1 block endoplasmic reticulum to Golgi transport and trigger disassembly of the Golgi apparatus. *J. Biol. Chem.* **269**, 1437-1448.

Davids, B. J., Reiner, D. S., Birkeland, S. R., Preheim, S. P., Cipriano, M. J., McArthur, A. G. and Gillin, F. D. (2006). A new family of giardial cysteine-rich non-VSP protein genes and a novel cyst protein. *PLoS ONE* **1**, e44.

Davis-Hayman, S. R. and Nash, T. E. (2002). Genetic manipulation of Giardia lamblia. *Mol. Biochem. Parasitol.* **122**, 1-7.

Davis-Hayman, S. R., Hayman, J. R. and Nash, T. E. (2003). Encystation-specific regulation of the cyst wall protein 2 gene in Giardia lamblia by multiple cis-acting elements. *Int. J. Parasitol.* **33**, 1005-1012.

Donaldson, J. G., Honda, A. and Weigert, R. (2005). Multiple activities for Arf1 at the Golgi complex. *Biochim. Biophys. Acta* **1744**, 364-373.

DuBois, K. N., Abodeely, M., Sakanari, J., Craik, C. S., Lee, M., McKerrow, J. H. and Sajid, M. (2008). Identification of the major cysteine protease of Giardia and its role in encystation. *J. Biol. Chem.* **283**, 18024-18031.

Elias, E. V., Quiroga, R., Gottig, N., Nakanishi, H., Nash, T. E., Neiman, A. and Lujan, H. D. (2008). Characterization of SNAREs determines the absence of a typical Golgi apparatus in the ancient eukaryote Giardia lamblia. *J. Biol. Chem* **283**, 35996-36010.

Feinstein, T. N. and Linstedt, A. D. (2007). Mitogen-activated protein kinase kinase 1-dependent Golgi unlinking occurs in G2 phase and promotes the G2/M cell cycle transition. *Mol. Biol. Cell* **18**, 594-604.

Feinstein, T. N. and Linstedt, A. D. (2008). GRASP55 regulates Golgi ribbon formation. *Mol. Biol. Cell* **19**, 2696-2707.

Gaechter, V., Schraner, E., Wild, P. and Hehl, A. B. (2008). The single dynamin family protein in the primitive protozoan Giardia lamblia is essential for stage conversion and endocytic transport. *Traffic* **9**, 57-71.

Gillin, F. D., Reiner, D. S. and McCaffery, J. M. (1996). Cell biology of the primitive eukaryote Giardia lamblia. *Annu. Rev. Microbiol.* **50**, 679-705.

Griffiths, G. (2000). Gut thoughts on the Golgi complex. *Traffic* **1**, 738-745.

Hager, K. M., Striepen, B., Tilney, L. G. and Roos, D. S. (1999). The nuclear envelope serves as an intermediary between the ER and Golgi complex in the intracellular parasite Toxoplasma gondii. *J. Cell Sci.* **112**, 2631-2638.

He, C. Y., Ho, H. H., Malsam, J., Chalouni, C., West, C. M., Ullu, E., Toomre, D. and Warren, G. (2004). Golgi duplication in Trypanosoma brucei. *J. Cell Biol.* **165**, 313-321.

Hehl, A. B., Marti, M. and Kohler, P. (2000). Stage-specific expression and targeting of cyst wall protein-green fluorescent protein chimeras in Giardia. *Mol. Biol. Cell* **11**, 1789-1800.

Heidtman, M., Chen, C. Z., Collins, R. N. and Barlowe, C. (2003). A role for Yip1p in COPII vesicle biogenesis. *J. Cell Biol.* **163**, 57-69.

Jarroll, E. L., Macechko, P. T., Steimle, P. A., Bulik, D., Karr, C. D., van Keulen, H., Paget, T. A., Gerwig, G., Kamerling, J., Vliegenthart, J. et al. (2001). Regulation of carbohydrate metabolism during Giardia encystment. *J. Eukaryot. Microbiol.* **48**, 22-26.

Jimenez-Garcia, L. F., Zavala, G., Chavez-Munguia, B., Ramos-Godinez Mdel, P., Lopez-Velazquez, G., Segura-Valdez Mde, L., Montanez, C., Hehl, A. B., Arguello-Garcia, R. and Ortega-Pierres, G. (2008). Identification of nucleoli in the early branching protist Giardia duodenalis. *Int. J. Parasitol.* **38**, 1297-1304.

Kuge, O., Dascher, C., Orci, L., Rowe, T., Amherdt, M., Plutner, H., Ravazzola, M., Tanigawa, G., Rothman, J. E. and Balch, W. E. (1994). Sar1 promotes vesicle budding from the endoplasmic reticulum but not Golgi compartments. *J. Cell Biol.* **125**, 51-65.

Lanfredi-Rangel, A., Attias, M., Reiner, D. S., Gillin, F. D. and De Souza, W. (2003). Fine structure of the biogenesis of Giardia lamblia encystation secretory vesicles. *J. Struct. Biol.* **143**, 153-163.

Lanoix, J., Ouwendijk, J., Lin, C. C., Stark, A., Love, H. D., Ostermann, J. and Nilsson, T. (1999). GTP hydrolysis by arf-1 mediates sorting and concentration of Golgi resident enzymes into functional COP I vesicles. *EMBO J.* **18**, 4935-4948.

Lloyd, D. and Harris, J. C. (2002). Giardia: highly evolved parasite or early branching eukaryote? *Trends Microbiol.* **10**, 122-127.

Losev, E., Reinke, C. A., Jellen, J., Strongin, D. E., Bevis, B. J. and Glick, B. S. (2006). Golgi maturation visualized in living yeast. *Nature* **441**, 1002-1006.

Lujan, H. D., Marotta, A., Mowatt, M. R., Sciaky, N., Lippincott-Schwartz, J. and Nash, T. E. (1995a). Developmental induction of Golgi structure and function in the primitive eukaryote Giardia lamblia. *J. Biol. Chem.* **270**, 4612-4618.

Lujan, H. D., Mowatt, M. R., Conrad, J. T., Bowers, B. and Nash, T. E. (1995b). Identification of a novel Giardia lamblia cyst wall protein with leucine-rich repeats. Implications for secretory granule formation and protein assembly into the cyst wall. *J. Biol. Chem.* **270**, 29307-29313.

Lujan, H. D., Mowatt, M. R., Byrd, L. G. and Nash, T. E. (1996). Cholesterol starvation induces differentiation of the intestinal parasite Giardia lamblia. *Proc. Natl. Acad. Sci. USA* **93**, 7628-7633.

Marti, M. and Hehl, A. B. (2003). Encystation-specific vesicles in Giardia: a primordial Golgi or just another secretory compartment? *Trends Parasitol.* **19**, 440-446.

Marti, M., Li, Y., Schraner, E. M., Wild, P., Kohler, P. and Hehl, A. B. (2003a). The secretory apparatus of an ancient eukaryote: protein sorting to separate export pathways occurs before formation of transient Golgi-like compartments. *Mol. Biol. Cell* **14**, 1433-1447.

Marti, M., Regos, A., Li, Y., Schraner, E. M., Wild, P., Muller, N., Knopf, L. G. and Hehl, A. B. (2003b). An ancestral secretory apparatus in the protozoan parasite Giardia intestinalis. *J. Biol. Chem.* **278**, 24837-24848.

Memon, A. R. (2004). The role of ADP-ribosylation factor and SAR1 in vesicular trafficking in plants. *Biochim. Biophys. Acta* **1664**, 9-30.

Morrison, H. G., McArthur, A. G., Gillin, F. D., Aley, S. B., Adam, R. D., Olsen, G. J., Best, A. A., Cande, W. Z., Chen, F., Cipriano, M. J. et al. (2007). Genomic minimalism in the early diverging intestinal parasite Giardia lamblia. *Science* **317**, 1921-1926.

Pelletier, L., Stern, C. A., Pypaert, M., Sheff, D., Ngo, H. M., Roper, N., He, C. Y., Hu, K., Toomre, D., Coppens, I. et al. (2002). Golgi biogenesis in Toxoplasma gondii. *Nature* **418**, 548-552.

Peyroche, A., Antonny, B., Robineau, S., Acker, J., Cherfils, J. and Jackson, C. L. (1999). Brefeldin A acts to stabilize an abortive ARF-GDP-Sec7 domain protein complex: involvement of specific residues of the Sec7 domain. *Mol. Cell* **3**, 275-285.

Reiner, D. S., McCaffery, J. M. and Gillin, F. D. (2001). Reversible interruption of Giardia lamblia cyst wall protein transport in a novel regulated secretory pathway. *Cell Microbiol.* **3**, 459-472.

Robbins, P. W. and Samuelson, J. (2005). Asparagine linked glycosylation in Giardia. *Glycobiology* **15**, 15G-16G.

Rossanese, O. W., Soderholm, J., Bevis, B. J., Sears, I. B., O'Connor, J., Williamson, E. K. and Glick, B. S. (1999). Golgi structure correlates with transitional endoplasmic

reticulum organization in Pichia pastoris and Saccharomyces cerevisiae. *J. Cell Biol.* **145**, 69-81.

Samuelson, J., Banerjee, S., Magnelli, P., Cui, J., Kelleher, D. J., Gilmore, R. and Robbins, P. W. (2005). The diversity of dolichol-linked precursors to Asn-linked glycans likely results from secondary loss of sets of glycosyltransferases. *Proc. Natl. Acad. Sci. USA* **102**, 1548-1553.

Saraiya, A. A. and Wang, C. C. (2008). snoRNA, a novel precursor of microRNA in Giardia lamblia. *PLoS Pathog.* **4**, e1000224.

Stefanic, S., Palm, D., Svard, S. G. and Hehl, A. B. (2006). Organelle proteomics reveals cargo maturation mechanisms associated with Golgi-like encystation vesicles in the early-diverged protozoan Giardia lamblia. *J. Biol. Chem.* **281**, 7595-7604.

Stephens, D. J. and Pepperkok, R. (2001). Illuminating the secretory pathway: when do we need vesicles? *J. Cell Sci.* **114**, 1053-1059.

Stephens, D. J., Lin-Marq, N., Pagano, A., Pepperkok, R. and Paccaud, J. P. (2000). COPI-coated ER-to-Golgi transport complexes segregate from COPII in close proximity to ER exit sites. *J. Cell Sci.* **113**, 2177-2185.

Struck, N. S., Herrmann, S., Schmuck-Barkmann, I., de Souza Dias, S., Haase, S., Cabrera, A. L., Treeck, M., Bruns, C., Langer, C., Cowman, A. F. et al. (2008). Spatial dissection of the cis- and trans-Golgi compartments in the malaria parasite Plasmodium falciparum. *Mol. Microbiol.* **67**, 1320-1330.

Sun, C. H. and Tai, J. H. (2000). Development of a tetracycline controlled gene expression system in the parasitic protozoan Giardia lamblia. *Mol. Biochem. Parasitol.* **105**, 51-60.

Sun, C. H., McCaffery, J. M., Reiner, D. S. and Gillin, F. D. (2003). Mining the Giardia lamblia genome for new cyst wall proteins. *J. Biol. Chem.* **278**, 21701-21708.

Tisdale, E. J., Bourne, J. R., Khosravi-Far, R., Der, C. J. and Balch, W. E. (1992). GTP-binding mutants of rab1 and rab2 are potent inhibitors of vesicular transport from the endoplasmic reticulum to the Golgi complex. *J. Cell Biol.* **119**, 749-761.

Touz, M. C., Nores, M. J., Slavin, I., Carmona, C., Conrad, J. T., Mowatt, M. R., Nash, T. E., Coronel, C. E. and Lujan, H. D. (2002). The activity of a developmentally regulated cysteine proteinase is required for cyst wall formation in the primitive eukaryote Giardia lamblia. *J. Biol. Chem.* **277**, 8474-8481.

Tovar, J., Leon-Avila, G., Sanchez, L. B., Sutak, R., Tachezy, J., van der Giezen, M., Hernandez, M., Muller, M. and Lucocq, J. M. (2003). Mitochondrial remnant organelles of Giardia function in iron-sulphur protein maturation. *Nature* **426**, 172-176.

Trucco, A., Polishchuk, R. S., Martella, O., Di Pentima, A., Fusella, A., Di Giandomenico, D., San Pietro, E., Beznoussenko, G. V., Polishchuk, E. V., Baldassarre, M. et al. (2004). Secretory traffic triggers the formation of tubular continuities across Golgi sub-compartments. *Nat. Cell Biol.* **6**, 1071-1081.

Warren, G. and Malhotra, V. (1998). The organisation of the Golgi apparatus. *Curr. Opin. Cell Biol.* **10**, 493-498.

Yang, X., Matern, H. T. and Gallwitz, D. (1998). Specific binding to a novel and essential Golgi membrane protein (Yip1p) functionally links the transport GTPases Ypt1p and Ypt31p. *EMBO J.* **17**, 4954-4963.